







One-dimensional magnetism in synthetic Pauflerite, β -VOSO₄

Diana Lucia Quintero-Castro ^{1,2,*}, Gøran J. Nilsen ^{1,3}, Katrin Meier-Kirchner,²
 Angelica Benitez-Castro,⁴ Gerrit Guenther ², Toshiro Sakakibara,⁵ Masashi Tokunaga,⁵
 Chidozie Agu ¹, Ipsita Mandal ^{1,6} and Alexander A. Tsirlin ⁷

¹Department of Mathematics and Physics, University of Stavanger, 4036 Stavanger, Norway

²Helmholtz Zentrum Berlin für Materialien und Energie, D-14109 Berlin, Germany

³ISIS Neutron and Muon Source, STFC Rutherford Appleton Laboratory, Didcot OX11 0QX, United Kingdom

⁴Laboratory for Magnetism and Advanced Materials, Universidad Nacional de Colombia, Manizales 17003, Colombia

⁵The Institute for Solid State Physics, The University of Tokyo, Kashiwa, Chiba 277-8581, Japan

⁶Institute of Nuclear Physics, Polish Academy of Sciences, 31-342 Kraków, Poland

⁷Felix Bloch Institute for Solid-State Physics, Leipzig University, 04103 Leipzig, Germany



(Received 19 December 2022; accepted 17 March 2023; published 17 April 2023)

We have synthesized single-crystal samples of β -VOSO₄ and fully characterized their magnetic properties. Our magnetic susceptibility, high field magnetization, and powder inelastic neutron scattering results are in excellent agreement with theoretical expressions for a one-dimensional spin-1/2 Heisenberg chain with an exchange parameter of 3.83(2) meV. *Ab initio* calculations identify the superexchange pathway, revealing that the spin-chain does not run along the expected crystallographic chain *a* direction but instead between V⁴⁺O₆ octahedra that are linked via SO₄ tetrahedra along the *b* axis. We do not detect any phase transition to a long-range magnetic order within our experimental conditions, indicating β -VOSO₄ is very close to an ideal one-dimensional magnetic system.

DOI: [10.1103/PhysRevMaterials.7.045003](https://doi.org/10.1103/PhysRevMaterials.7.045003)

I. INTRODUCTION

Low-dimensional Heisenberg systems are a fertile testing ground which offer well-recognized model materials [1,2], exact analytical solutions [3,4], multiple experimental predictions [5,6], newly proposed quantum simulations [7], and technological applications, such as quantum spin transistors [8]. Many low-dimensional Heisenberg magnets are d^1 V⁴⁺ spin $s = 1/2$ ($s - 1/2$) oxides. In these compounds, the crystal field environment, with a distinctive short V-O bond, lifts the degeneracy of the t_{2g} orbitals, hence quenching the orbital magnetic moment. The lowest-energy half-filled d_{xy} orbital lies in the plane perpendicular to the short bond, where it can overlap with oxygen orbitals, creating superexchange paths that give rise to a dominant planar antiferromagnetic (AFM) interaction, and hence to low-dimensional spin systems [9–14].

β -VOSO₄ was first synthesized in 1928 by Sieverts and Müller [15] by the reduction of V⁵⁺ in sulfuric acid. Later, in 2007, it was discovered among volcanic products of the Tolbachik volcano in Kamchatka, Russia [16]. Vanadyl-based compounds like β -VOSO₄ and its hydro-oxosulfate modifications attract the interest of chemists and biologists due to their potential applications in catalysis and the management of diabetes [17,18]. β -VOSO₄ crystallizes in the *Pnma* orthorhombic group and its structure represents a three-dimensional framework built up of distorted V⁴⁺O₆ octahedra

and (SO₄)²⁻ tetrahedra. Recent crystallographic studies have revealed 2% of correlated defects in the here investigated synthetic crystals [19]. These are linked to an inversion of the short-long V-O distance pairs and form thin layers with a negative interlayer correlation, randomly destroying the alternation of the V-O bonding pattern along the *b* axis. Figure 1(a) shows a representation of the crystal structure of β -VOSO₄ following Ref. [19] showing a 98% occupation of the vanadium site at (0.334, 0.25, 0.2675).

Previous studies of the magnetism in β -VOSO₄ through magnetic susceptibility measurements report long-range antiferromagnetic order [20] and ferrimagnetic behavior [21]. Here, we revise these previously published interpretations in light of data from newly grown mm-sized single crystals. We characterize the magnetic properties, through magnetic susceptibility, high field magnetization measurements and powder inelastic neutron scattering (INS). The INS data shows clear gapless spinons with a continuum spanning up to 12 meV. These data are compared to calculations of the spinon continuum of the one-dimensional (1D) Heisenberg chain. Reasonable agreement is found for $J_1 = 3.83(2)$ meV, with the dominant exchange running along the *b* direction within the exchange path predicted by our *ab initio* calculations. We find the effect of interchain couplings to be negligible and confirm the system to be a 1D $s=1/2$ Heisenberg chain magnet.

II. EXPERIMENTAL AND CALCULATION DETAILS

Single crystal samples of β -VOSO₄ were synthesized through the reaction: $V_2O_5 + 2H_2SO_4 \rightarrow 2\beta\text{-VOSO}_4 + 2H_2O$

*diana.l.quintero@uis.no

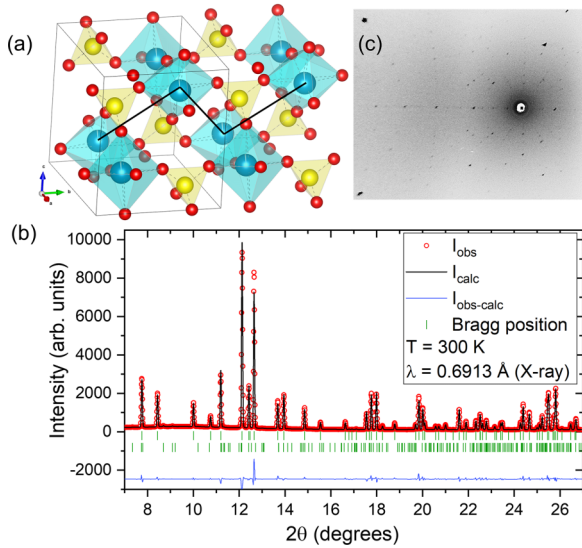


FIG. 1. (a) Graphic representation of the crystal structure of β -VOSO₄ created using VESTA [22]. SO₄ tetrahedra are represented in yellow, while V⁴⁺O₆ octahedra are blue showing a partial occupation of the V⁴⁺ site following Ref. [19]. Oxygen ions are in red. The black line represents the main magnetic exchange interaction as described in the sessions below. (b) X-ray diffraction pattern of β -VOSO₄ at 300 K along with its Rietveld refinement. Experimental data in red, calculated pattern in black, and difference in blue. There are two sets of Bragg positions; above, the positions related to the β -VOSO₄ structure and the ones below are due to the VH₆SO₈ impurity. (c) X-ray Laue image with the beam parallel to the *c* axis for the sample used for magnetometry.

+ 0.5O₂, following Ref. [15]. A solution of 3 g of V₂O₅ and 100 ml H₂SO₄ was heated up just below the boiling point of H₂SO₄ at 290°C in a conical flask for a maximum period of 3 months. A fractionating column was used to condense all vapors. Slow heating and cooling rates of 135°C/h and 30°C/h were used, respectively. All products were washed multiple times in an ice-water bath and dried at 110°C for 12 h. Thermogravimetric analysis was performed to ensure no water was left in the samples. These results (not shown here) were in agreement with those of Paufler *et al.* [23]. Our longest reaction of 3 months allowed the growth of needle-like single crystals as long as 6 mm of a green color. X-ray Laue diffraction [Fig. 1(c)] was used to confirm the crystallinity of the samples. Powder samples were produced by grinding the single crystals. Indications of a small amount of the impurity phase VH₆SO₈ (space group *P2*₁/*c*) were found in x-ray powder diffraction data. Figure 1(b) shows the x-ray powder diffraction data along with its refinement. This data was acquired using the BM01 diffractometer at SNBL-ESRF using a wavelength of 0.6913 Å. The impurity is contained in the powder matrix where the crystals grow (not in the single crystals). The content varies in the powder sample but it amounts to less than 1% of the total mass.

A single crystal sample of mass 7.021 mg was used to measure magnetic susceptibility using a Quantum Design superconducting quantum interference device magnetometer. These measurements were carried out in both zero-field and field-cooled modes with a magnetic field of 0.5 T applied

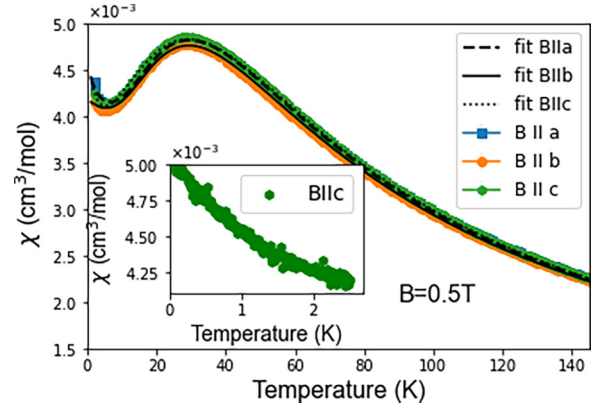


FIG. 2. Static susceptibility data for a magnetic field of 0.5 T applied along each main crystallographic direction, displayed along with the fitted expression for a $s - 1/2$ uniform Heisenberg chain given by Eq. (50) in Ref. [28]. Details of the low-temperature range (85 mK to 2.5 K) with field applied along the *c* axis are shown in the inset.

along the three main crystallographic directions. The temperature range for the measurements was 2–300 K. This magnetometer was also used to measure magnetization in a single crystal of mass 27.97 mg with magnetic fields up to 5 T applied along the *a* axis at 4.2 K. This measurement was performed in order to calibrate the magnetic moment measured in the pulsed high magnetic fields using an induction method at the International MegaGauss Science Laboratory. This measurement was also performed at 4.2 K on the same sample and fields up to 66.3 T were achieved. Additionally, a homemade high sensitivity magnetometer was used to measure the magnetic susceptibility in the temperature range 0.085–2.5 K with a magnetic field of 0.5 T applied along the *c* axis [24].

INS experiments were performed on a polycrystalline sample of mass 2.614 g in an annular shape Al-foil holder, at 3 K using the direct geometry neutron ToF instrument NEAT at HZB [25]. Measurements were performed with neutrons of incident wavelengths of 2, 3 and 5 Å (incident energies 20.45, 9.09, and 3.27 meV, respectively).

Density-functional theory (DFT) band-structure calculations were performed in the FPLO code [26] using the generalized gradient approximation (GGA) for the exchange correlation potential [27]. A dense \mathbf{k} mesh with up to 343 points in the symmetry-irreducible part of the Brillouin zone was used.

III. RESULTS AND CALCULATIONS

A. Static susceptibility and magnetization

The magnetic static susceptibility of β -VOSO₄ with magnetic field of 0.5 T applied along the main three crystallographic axes is shown in Fig. 2. The three curves are slightly different, suggesting a weakly anisotropic *g* tensor. The Curie-Weiss temperatures and Curie constants obtained from a fit to the Curie-Weiss law above 150 K are listed in Table I. The former temperatures are between −34.5 and −39.4 K, suggesting dominant AFM interactions. Zero-field-cooled and field-cooled measurements were done, and showed no sign of

TABLE I. Parameters obtained by fitting the susceptibility data both to the Curie-Weiss law (above 150 K and resulting C and θ_{CW}) and to Eq. (50) in Ref. [28] in the whole temperature range.

	C (cm ³ /mol K)	θ_{CW} (K)	J_{1D} (meV)	g	C_{imp} (cm ³ /mol K)	$\theta_{CW-\text{imp}}$ (K)	χ_0 (cm ³ /mol)
B \parallel a	0.4034(3)	-34.5(2)	4.107(5)	2.006(7)	0.004(1)	-3.8(2)	$3.6(1) \times 10^{-5}$
B \parallel b	0.4103(2)	-39.4(2)	4.108(6)	1.979(1)	0.006(4)	-7.9(5)	$6.4(1) \times 10^{-5}$
B \parallel c	0.4056(4)	-35.0(3)	4.11(5)	2.010(7)	0.005(2)	-6.8(4)	$3.1(1) \times 10^{-5}$

any hysteresis processes in the measured ranges (not shown here). All three susceptibility plots show a broad maximum centered at ≈ 29 K. Such a susceptibility curve is characteristic of low-dimensional magnets. The inset in Fig. 2 shows the magnetic susceptibility for magnetic fields applied along the c axis and temperatures down to 0.085 K. No sign of a transition to a long-range magnetic ordered state was detected within this experimental range.

Assuming the hypothesis that β -VOSO₄ is an $s - 1/2$ antiferromagnetic Heisenberg chain system, we use the expression calculated by Johnston *et al.* [28] [Eqs. (30) and (31)], for the characteristic temperature of the maximum of the magnetic susceptibility $T_{\chi_{\text{max}}} = 0.640851|J_{1D}|/k_B$. From this expression, we can estimate an intrachain interaction (J_{1D}) of 3.9 meV for fields along the a and c directions and 3.78 meV for fields along the b axis. Furthermore, by setting the g factors to those reported in Ref. [29], we obtain $\chi_{\text{max}} T_{\chi_{\text{max}}} = 0.035477 g^2 \frac{\text{cm}^3 \text{K}}{\text{mol}}$ for fields along the a axis, $\chi_{\text{max}} T_{\chi_{\text{max}}} = 0.037857 g^2 \frac{\text{cm}^3 \text{K}}{\text{mol}}$ for the b axis and $\chi_{\text{max}} T_{\chi_{\text{max}}} = 0.035744 g^2 \frac{\text{cm}^3 \text{K}}{\text{mol}}$ for the c axis. These values are very close to the theoretical value for a $s - 1/2$ AF uniform Heisenberg chain where $\chi_{\text{max}} T_{\chi_{\text{max}}} = 0.0353229(3) g^2 \frac{\text{cm}^3 \text{K}}{\text{mol}}$ [28].

Giving these similarities, we proceed to fit the data to the mean-field approximation for the magnetic susceptibility of an $s - 1/2$ uniform ($\alpha = 1$) Heisenberg chain with an intra-chain interaction (J_{1D}), following Eq. (50) in Ref. [28]. The total fitting function also includes a Curie-Weiss law term to account for the contribution of paramagnetic impurities [$C_{\text{imp}}/(T - \theta_{CW-\text{imp}})$], which dominate the data below 7 K and a background susceptibility (χ_0) to account for core diamagnetism and van Vleck contributions. All resultant parameters are listed in Table I. The impurity Curie constant amounts to 1–1.45% of the β -VOSO₄ Curie constant values. These paramagnetic impurities could be well linked to the 2% defect planes reported in Ref. [19]. The g values were also extracted using the fit to Eq. (50) in Ref. [28]. These values are very close to 2 but are slightly bigger than those typically reported for V⁴⁺ [30]. In comparison the g values extracted from the $\chi_{\text{max}} T_{\chi_{\text{max}}}$ expressions are 1.991, 1.947, 1.998 for fields parallel to each main crystallographic axis.

The high field magnetization of β -VOSO₄ at 4.2 K for fields applied along the a axis is shown in Fig. 3. The magnetization increases with H following the function:

$$M = M_{\text{sat}} \left(1 - \sqrt{1 - (H/H_{\text{sat}})} \right), \quad (1)$$

where M_{sat} is the saturation magnetization per V⁴⁺ ion, H is magnetic field and H_{sat} is the saturation field, 68.46 T, following the description given in Ref. [31]. The red dotted line in Fig. 3 corresponds to this equation with $J_{1D} = 4.107$ meV and $g = 2.006$ obtained by the susceptibility fit for the a axis. No

fitting procedure was done in the case of the magnetization modeling. The magnetic exchange interaction extracted from the susceptibility follows well the magnetization below 20 T after which it deviates given a much larger saturation field. The experimental saturation field is expected to be at 70.7 T just above the highest available magnetic field for this experiment. Calculation of the magnetization using the magnetic exchange interaction found in the analysis of the inelastic neutron scattering (as described in the section Magnetic excitations) is also shown in the figure as a black dashed line. This value provides a much more accurate description of the magnetization in the whole magnetic field range.

B. *Ab initio* calculations

To see which of the many possible exchange terms may be relevant in the case of β -VOSO₄, we first perform *ab initio* calculations, where we consider magnetic exchange couplings J_{ij} entering the spin Hamiltonian:

$$\mathcal{H} = \sum_{\langle ij \rangle} J_{ij} S_i S_j. \quad (2)$$

with the summation running over lattice bonds $\langle ij \rangle$. The exchange parameters J_{ij} were extracted using two complementary approaches. On one hand, we calculate hopping integrals between the V 3d states using Wannier functions constructed for the uncorrelated (GGA) band structure, and introduce these hoppings into the Kugel-Khomskii model that

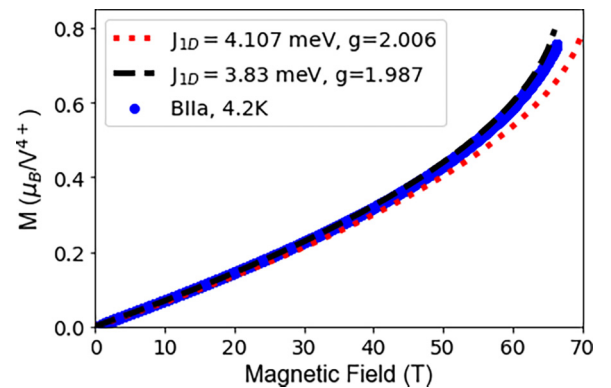


FIG. 3. Magnetization per V⁴⁺ ions as a function of applied magnetic field, performed using a pulsed magnet at 4.2 K and field applied parallel to the a axis (blue). The red dashed line corresponds to Eq. (1) using the magnetic exchange interactions obtained from the susceptibility data without any fitting. The black dashed line corresponds to the calculated using the same equation but with the magnetic exchange interaction derived from the fit to the inelastic neutron scattering data and the published g factor for V⁴⁺ [30].

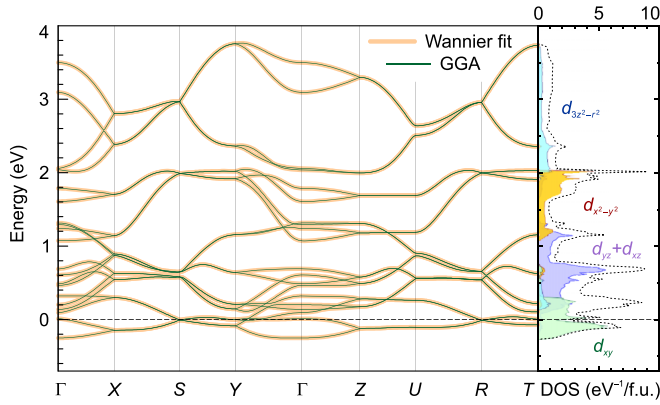


FIG. 4. GGA bands and their Wannier fit for extracting the hopping parameters. The right panel shows orbital-resolved contributions to the density of states and indicates the predominance of the d_{xy} states near the Fermi level. The k path is defined as $\Gamma(0, 0, 0)$, $X(\frac{1}{2}, 0, 0)$, $S(\frac{1}{2}, \frac{1}{2}, 0)$, $Y(0, \frac{1}{2}, 0)$, $Z(0, 0, \frac{1}{2})$, $U(\frac{1}{2}, 0, \frac{1}{2})$, $R(\frac{1}{2}, \frac{1}{2}, \frac{1}{2})$, and $T(0, \frac{1}{2}, \frac{1}{2})$.

then delivers the magnetic exchange couplings as follows [10,13]:

$$J_{ij} = \frac{(4t_{ij}^{(nm)})^2}{U_{\text{eff}}} - \sum_m \frac{4(t_{ij}^{(nm)})^2 J_{\text{eff}}}{(U_{\text{eff}} + \Delta_m)(U_{\text{eff}} - J_{\text{eff}} + \Delta_m)}, \quad (3)$$

where the first and second terms stand for the antiferromagnetic (J_{ij}^{AFM}) and ferromagnetic (J_{ij}^{FM}) contributions, respectively. Here, $U_{\text{eff}} = 4$ eV is the effective on-site Coulomb repulsion and $J_{\text{eff}} = 1$ eV is the effective Hund's coupling in the V $3d$ shell [10,11]. The hoppings $t_{ij}^{(nm)}$ are between the half-filled states of vanadium, whereas $t_{ij}^{(nm)}$ involve the empty states m , and $\Delta_m = E_m - E_n$ is the crystal-field splitting. GGA bands and their Wannier fit are shown in Fig. 4. Alternatively, we obtain the exchange couplings by a mapping procedure [32,33] using total energies of collinear spin configurations evaluated within DFT+U, where correlation effects in the V $3d$ shell are treated on the mean-field level with the on-site Coulomb repulsion $U_d = 4$ eV, Hund's coupling $J_d = 1$ eV, and atomic-limit flavor of the double-counting correction [34,35].

In the absence of correlations, the GGA band structure of β -VOSO₄ is metallic and features a broad V $3d$ band that spans the energy range between -0.3 and 3.8 eV. The lower part of this band is dominated by the half-filled d_{xy} states. Here, we define the local coordinate system in such a way that the z axis points along the short (vanadyl) bond of the VO₆ octahedron, whereas x and y point along the longer V-O bonds that are approximately perpendicular to it. Then, z is close to the a direction and thus nearly parallel to the structural chains in β -VOSO₄. Only the d_{xy} states are half-filled, and all other $3d$ states of vanadium are empty, as typical for V⁴⁺ [13,14,33].

Both ferro- and antiferromagnetic contributions to the exchange couplings obtained from Eq. (3), as well as total exchange couplings J_{ij} obtained by the mapping procedure, are listed and represented graphically in Fig. 5. Long-range interaction terms not included in this table are well below

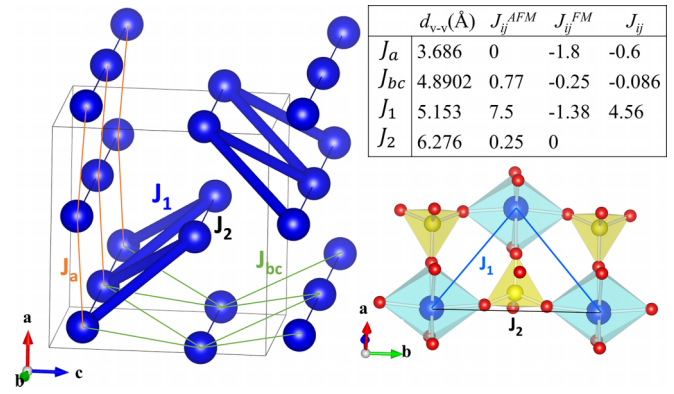


FIG. 5. Exchange couplings in β -VOSO₄. The crystal representations were created with VESTA [22]. Blue balls represent vanadium ions, yellow is sulfur, and red is oxygen. The values of J_{ij}^{AFM} and J_{ij}^{FM} are listed in the inserted table in meV units. These are derived from the Kugel-Khomskii model, Eq. (3), and show relative contributions of different superexchange mechanisms. Total exchange couplings are J_{ij} obtained by the DFT+U mapping analysis and may be different from J^{AFM} .

0.008 meV and can be safely neglected. The nearest-neighbor coupling along the structural chains (J_a) is relatively weak and ferromagnetic, while the strongest coupling, $J_1 \approx 4.3$ meV, runs between the VO₆ octahedra that are linked via two SO₄ tetrahedra (see Fig. 5). Such a coupling regime is common for V⁴⁺ phosphates, arsenates, and other compounds with tetrahedral polyanions [12,36]. On the one hand, double tetrahedral bridges create a V-O...O-V superexchange pathway that are reasonably efficient despite the large V-V separation of more than 5 Å. On the other hand, the position of the half-filled d_{xy} orbital in the plane perpendicular to the structural chain prevents the xy - xy hopping (and, thus, an antiferromagnetic interaction) for the shorter V-V separation along the chain and renders J_a weakly ferromagnetic [36,37]. The remaining couplings J_2 and J_{bc} are much weaker as each of them is mediated by single SO₄ tetrahedron with a less efficient orbital overlap [38]. Orbital directions can be depicted similarly to those reported in Ref. [10].

The DFT+U calculations described above were performed for the supercells doubled along the b and c directions without including the distortion reported in Ref. [19]. To account for the effect of structural disorder, we considered two possible configurations, ++++ and +-+- in the notation of Ref. [19]. Crystal structures of both configurations were optimized on the GGA level, and exchange couplings were calculated by the DFT+U mapping procedure. We found $J_1 = 3.53$ meV and $J_a = -0.6$ meV for the ++++ configuration vs $J_1 = 3.7$ meV and $J_a = -0.77$ meV for the +-+- configuration. These very minute changes suggest that structural disorder has a minor effect on magnetism.

C. Magnetic excitations

The dynamical structure factors $S(|Q|, \Delta E)$ of β -VOSO₄ collected at 3 K with neutron wavelengths of 2 and 3 Å ($E_i = 20.45, 9.09$ meV, respectively) are shown in Figs. 6(a) and 6(b). Magnetic scattering is clearly evident at

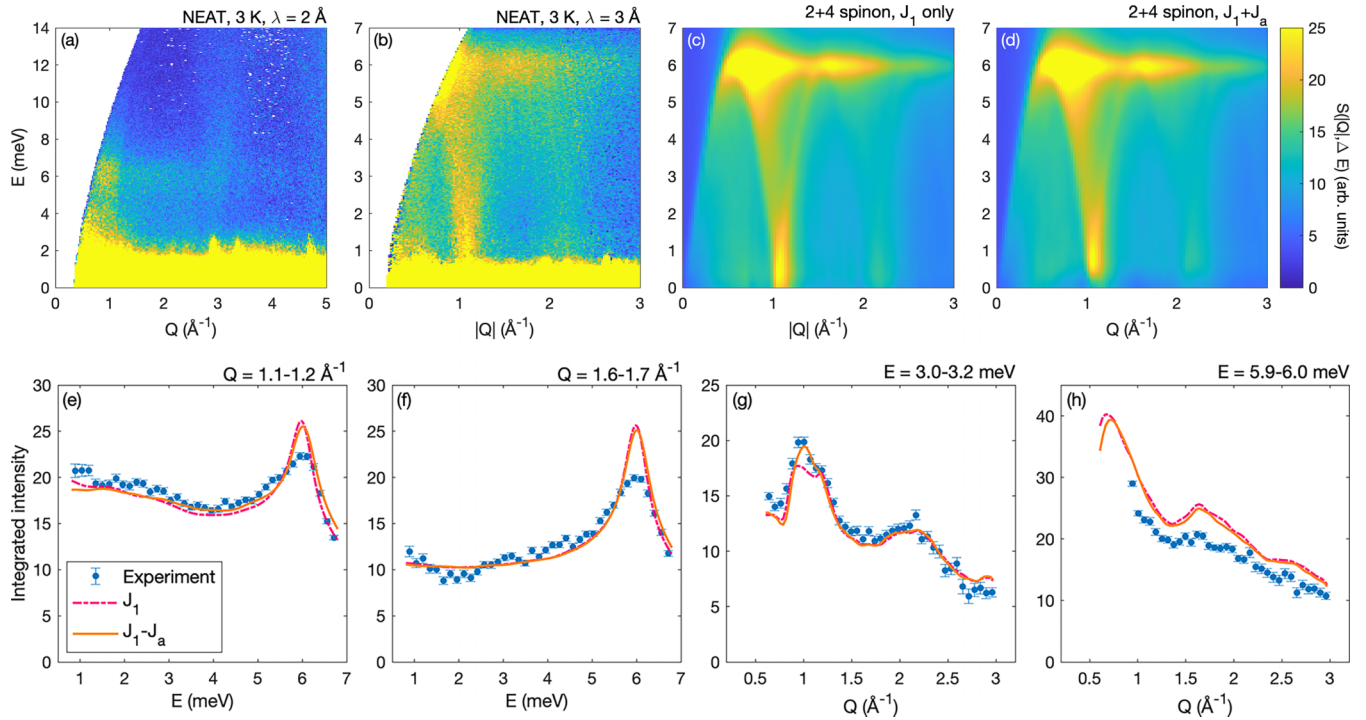


FIG. 6. (a), (b) Experimental $S(Q, \Delta E)$ for β -VOSO₄ at 3 K measured at neutron wavelengths $\lambda = 2 \text{ \AA}$ and 3 \AA on the NEAT spectrometer. (c), (d) Calculated $S(Q, \Delta E)$ for the J_1 -only (isolated chain, (c) and $J_1 + J_a$ (d) models. The model parameters are given in the text. (e)–(h) Constant- Q (e), (f) and ΔE (g), (h) cuts through the experimental 3 \AA data. Corresponding cuts through the calculated $S(Q, \Delta E)$ are indicated by red dot-dashed (J_1 only) and orange solid ($J_1 - J_a$) lines. The intensity is overestimated by around 20% at 6 meV (h).

low $|Q|$, dispersing from $|Q_0| \sim 1.05 \text{ \AA}^{-1}$ and extending in energy up to around 10 meV [Fig. 6(a)], with a sharp peak at $\Delta E \sim 6 \text{ meV}$. Weaker magnetic intensity is also observed near the elastic line around $|Q| \sim 0.6$ and 2 \AA^{-1} . Overall, the spectrum is reminiscent of powder data from other one-dimensional systems, like $\text{KTi}(\text{SO}_4)_2$ [39], $\text{Sr}_3\text{CuPtO}_6$ [40] and KMoOP_2O_7 [41]. The observed $|Q_0|$ is close to the double- $(\text{SO}_4)^{2-}$ -bridged zig-zag chains that run along the b axis (Fig. 5) in agreement with the *ab initio* calculations.

To further confirm the hypothesis that the experimental data can be reproduced assuming one-dimensional zig-zag chains along b , we compare our experimental data to the total dynamical structure factor $S_{1d}(Q_y, \Delta E)$ for the 2- and 4-spinon continua calculated using the Bethe ansatz [5]. To do this, the theoretical $S_{1d}(Q, \Delta E)$ is first recalculated due to the strong deviation of the chains from linearity and the resulting folding of the Brillouin zone. From the orthorhombic symmetry of the material, the folded $S(\mathbf{Q}, \Delta E)$ is expressed as

$$\begin{aligned}
 S(\mathbf{Q}, \Delta E) = & \cos^2(Q_x \delta_x) \cos^2(Q_z \delta_z) S_{1d}(\mathbf{Q}, \Delta E) \\
 & + \cos^2(Q_x \delta_x) \sin^2(Q_z \delta_z) S_{1d}(\mathbf{Q} + (110), \Delta E) \\
 & + \sin^2(Q_x \delta_x) \cos^2(Q_z \delta_z) S_{1d}(\mathbf{Q} + (111), \Delta E) \\
 & + \sin^2(Q_x \delta_x) \sin^2(Q_z \delta_z) S_{1d}(\mathbf{Q} + (011), \Delta E).
 \end{aligned} \quad (4)$$

Here, $S_{1d}(\mathbf{Q}, \Delta E)$ represents the linear chain 2- and 4-spinon dynamical structure factor shifted by a \mathbf{Q} -dependent lattice vector from the antiferromagnetic zone center (010), and $\delta_x = 0.1615$ and $\delta_z = 0.2353$ are the offsets of the V^{4+}

position $(\delta_x, \frac{1}{4}, \delta_z)$ from that which would generate a perfectly linear chain: $(0, \frac{1}{4}, 0)$. Following folding, the theoretical data is powder averaged, yielding $S(|Q|, \Delta E)$, shown in Fig. 6(c). The correct zone-boundary energy, corresponding to the maximum in ΔE at 6 meV, is recovered for an intrachain coupling $J_1 = 3.83(2) \text{ meV}$, and most details of the spectrum, including the weak intensities away from the main branch of the continuum are also reproduced ($\chi^2 = \sum (Y_{\text{obs}} - Y_{\text{calc}})^2 = 5.3$) for 6 constant- $|Q|$ cuts through $S(|Q|, \Delta E)$. On the other hand, the intensity at the zone-boundary energy is somewhat overestimated. This reduction in intensity is consistent with the presence of interchain couplings, as seen, for example, in the case of Cs_2CuX_4 ($X = \text{Cl}, \text{Br}$) [42]. This single J_1 value was used to calculate the magnetization using the Fisher and Bonner expression as previously described. As neutron scattering measurements are not affected by the g factor, the ESR literature g factor of 1.987 was used for this calculation [30]. Figure 3 shows the calculation as a black dashed line, again no fitting procedure was used. This comparison shows that the single magnetic intra-chain coupling of $J_1 = 3.83(2) \text{ meV}$ is a highly accurate value for β -VOSO₄.

The predictions from our *ab initio* calculations suggest that the dominant exchange beyond J_1 is J_a , while J_{bc} , and J_2 are somewhat smaller. Therefore, we performed fits of the dynamical structure factor $S(|Q|, \Delta E)$ for the J_1 - J_a model. This was done following the random phase approximation-style approach in Ref. [43], from which $S(\mathbf{Q}, \Delta E)$ is given by the following expression:

$$\frac{S_{1d}(Q_y, \Delta E)}{[1 + J'(\mathbf{Q})\chi'(Q_y, \Delta E)]^2 + [J''(\mathbf{Q})\chi''(Q_y, \Delta E)]^2}, \quad (5)$$

where $S_{1d}(Q_y, \Delta E)$ is defined as above and

$$J'(\mathbf{Q}) \simeq J_a \cos(Q_x/2) \cos(Q_z/2), \quad (6)$$

where the Fourier components for the further neighbor couplings correspond to that of the straight chain. It is necessary to normalize $S_{1d}(Q_y, \Delta E)$ such that $\int_0^{2\pi} \int_0^\infty S_{1d}(k_y, \Delta E) d\Delta E dk_y = 1$ for the exchanges extracted from Eq. (5) to be physically meaningful. The imaginary and real dynamical susceptibilities $\chi''(Q_y, \Delta E)$ and $\chi'(Q_y, \Delta E)$ were calculated using $S_{1d}(Q_y, \Delta E) = \chi''(k_y, \Delta E)/\pi$ and a numerical Kramers-Kronig transformation, respectively. Finally, Brillouin zone folding was accounted for before powder averaging to obtain $S(|Q|, \Delta E)$. Due to the time-consuming nature of this procedure, the fitting was performed using six constant- $|Q|$ cuts through the data rather than the full data set. The optimization was carried out using the particle swarm method, and a single constant was added to all cuts to account for the instrumental background. The fit to the $J_1 - J_a$ model yielded a slight reduction in χ^2 from 5.3 (for the J_1 only model) to 5.1, and a small $J_a = 0.2(1)\text{meV}$ and nearly unchanged $J_1 = 3.81(2)\text{meV}$ [Figs. 6(d)–6(h)]. The inclusion of terms beyond J_a did not result in any further improvements to the fit. Dzyaloshinskii-Moriya interactions could be further consider in the model as these are allowed due to the 2% crystallographic disorder and this is the scope of a future work.

IV. CONCLUSIONS

Our results show that the spin chains in $\beta\text{-VOSO}_4$ are formed by doubly $(\text{SO}_4)^{2-}$ -bridged chains along the b direction that do not coincide with the structural chains of the V^{4+}O_6 octahedra. These spin chains are magnetically coupled by the magnetic exchange interaction $J_1 = 3.83$ meV. This is

a common occurrence in V^{4+} compounds due to the nature of their half-filled magnetic orbital [44–46]. J_2 is the second neighbor coupling along the spin chain and it is at least one order of magnitude weaker than J_1 . It may be responsible for a weak frustration therein, although it is by far insufficient to open a spin gap, which was indeed not detected in any of our measurements. The coupling J_a links the spin chains into a three-dimensional network but with low connectivity as there are two such couplings per vanadium site, as opposed to the four interchain couplings per site assumed in a standard quasi-1D antiferromagnet. The remaining discrepancy between the modeled INS intensity and the experimental data at ~ 6 meV likely has a different origin, the investigation of which must await the availability of larger single crystals. The weak connectivity of the spin chains suggests that the Néel temperature of $\beta\text{-VOSO}_4$ could be quite low. Indeed, we do not detect any magnetic order down to 0.085 K within the used experimental settings. We do not detect any effect of the reported crystallographic disorder in the magnetic properties of $\beta\text{-VOSO}_4$, other than possibly a finite amount of paramagnetic impurities.

ACKNOWLEDGMENTS

We thank M. Reehius, B. Lake, D. Chernyshov, and C. Fuller for fruitful discussions as well as P. Karen for initial XRD results. Additional thanks to Helmholtz Zentrum Berlin for supporting A.B.-C. during this project through the summer student program. This work is based on experiments performed at the research reactor BER-II at the Helmholtz Zentrum Berlin, Germany, ISIS neutron and muon source in Rutherford Appleton Laboratory and Swiss-Norwegian Beamlines, at the ESRF. Collaboration with the Solid State Institute at the University of Tokyo was possible thanks to travel grant YYF given by the University of Stavanger to D. Q.-C..

-
- [1] N. Motoyama, H. Eisaki, and S. Uchida, Magnetic Susceptibility of Ideal Spin 1/2 Heisenberg Antiferromagnetic Chain Systems, Sr_2CuO_3 and SrCuO_2 , *Phys. Rev. Lett.* **76**, 3212 (1996).
 - [2] B. Lake, D. A. Tennant, C. Frost, and S. Nagler, Quantum criticality and universal scaling of a quantum antiferromagnet, *Nat. Mater.* **4**, 329 (2005).
 - [3] H. Bethe, Zur Theorie der Metalle: I. Eigenwerte und Eigenfunktionen der linearen Atomkette, *Eur. Phys. J. A* **71**, 205 (1931).
 - [4] S. Pati, S. Ramasesha, and D. Sen, Low-lying excited states and low-temperature properties of an alternating spin-1-spin-1/2 chain: A density-matrix renormalization-group study, *Phys. Rev. B* **55**, 8894 (1997).
 - [5] J.-S. Caux and R. Hagemans, The four-spinon dynamical structure factor of the Heisenberg chain, *J. Stat. Mech.* (2006) P12013.
 - [6] K. Povarov, T. Soldatov, R. Wang, A. Zheludev, A. Smirnov, and O. Starykh, Electron Spin Resonance of the Interacting Spinon Liquid, *Phys. Rev. Lett.* **128**, 187202 (2022).
 - [7] Q. Li, J. Cui, and W. Li, Detecting confined and deconfined spinons in dynamical quantum simulations, *Phys. Rev. Res.* **4**, 013193 (2022).
 - [8] O. Marchukov, A. Volosniev, M. Valiente, D. Petrosyan, and N. Zinner, Quantum spin transistor with a Heisenberg spin chain, *Nat. Commun.* **7**, 13070 (2016).
 - [9] Y. Savina, O. Bludov, V. Pashchenko, S. Gnatchenko, P. Lemmens, and H. Berger, Magnetic properties of the antiferromagnetic spin-1/2 chain system $\beta\text{-TeVO}_4$, *Phys. Rev. B* **84**, 104447 (2011).
 - [10] A. Tsirlin, O. Janson, and H. Rosner, Unusual ferromagnetic superexchange in CdVO_3 : The role of Cd, *Phys. Rev. B* **84**, 144429 (2011).
 - [11] A. Tsirlin and H. Rosner, *Ab initio* modeling of Bose-Einstein condensation in $\text{Pb}_2\text{V}_3\text{O}_9$, *Phys. Rev. B* **83**, 064415 (2011).
 - [12] U. Arjun, K. Ranjith, B. Koo, J. Sichelschmidt, Y. Skourski, M. Baenitz, A. Tsirlin, and R. Nath, Singlet ground state in the alternating spin-1/2 chain compound NaVOAsO_4 , *Phys. Rev. B* **99**, 014421 (2019).

- [13] V. Mazurenko, F. Mila, and V. Anisimov, Electronic structure and exchange interactions of $\text{Na}_2\text{V}_3\text{O}_7$, *Phys. Rev. B* **73**, 014418 (2006).
- [14] M. Korotin, I. Elfimov, V. Anisimov, M. Troyer, and D. Khomskii, Exchange Interactions and Magnetic Properties of the Layered Vanadates CaV_2O_5 , MgV_2O_5 , CaV_3O_7 , and CaV_4O_9 , *Phys. Rev. Lett.* **83**, 1387 (1999).
- [15] A. Sieverts and E. Mueller, Vanadinverbindungen und siedende Schwefelsäure, *Z. Anorg. Allg. Chem.* **173**, 313 (1928).
- [16] S. Krivovichev, L. Vergasova, S. Britvin, S. Filatov, V. Kahlenberg, and V. Ananiev, Pauflerite, $\beta\text{-VO}(\text{SO}_4)$, a new mineral species from the Tolbachik Volcano, Kamchatka Peninsula, Russia, *Canadian Mineralogist.* **45**, 921 (2007).
- [17] A. Goc, Biological activity of vanadium compounds, *Open Life Sci.* **1**, 314 (2006).
- [18] H. M. Oskooie, M. Heravi, and Y. Sh, Vanadyl Sulfate ($\text{VOSO}_4 \cdot 3\text{H}_2\text{O}$). An efficient catalyst for acylation of alcohols and phenols under solvent free condition, *J. Chin. Chem. Soc.* **55**, 713 (2008).
- [19] C. Fuller, D. L. Quintero-Castro, A. Bosak, V. Dyadkin, and D. Chernyshov, Correlated disorder and crystal structure of $\beta\text{-VOSO}_4$, *Acta Cryst. Sec. B* **78**, 842 (2022).
- [20] J. Longo and R. Arnott, Structure and magnetic properties of VOSO_4 , *J. Solid State Chem.* **1**, 394 (1970).
- [21] G. Villeneuve, L. Lezama, and T. Rojo, Magnetic properties of monohydrate and anhydrous vanadyl sulfates, *Mol. Cryst. Liq. Cryst.* **176**, 495 (1989).
- [22] K. Momma and F. Izumi, VESTA3 for three-dimensional visualization of crystal, volumetric and morphology data, *J. Appl. Cryst.* **44**, 1272 (2011).
- [23] P. Paufler, S. Filatov, R. Bubnova, and M. Krzhizhanovskaya, Synthesis and thermal behaviour of pauflerite, $\beta\text{-VOSO}_4$, and its α -modification, *Z. Kristallogr. Cryst. Mater.* **229**, 725 (2014).
- [24] Y. Shimizu, Y. Kono, T. Sugiyama, S. Kittaka, Y. Shimura, A. Miyake, D. Aoki, and T. M. Sakakibara, Development of high-resolution capacitive Faraday magnetometers for sub-Kelvin region, *Rev. Sci. Instrum.* **92**, 123908 (2021).
- [25] M. Russina, G. Guenther, V. Grzimek, R. Gainov, M. Schlegel, L. Drescher, T. Kaulich, W. Graf, B. Urban, A. Daske, K. Grotjahn, R. Hellhammer, G. Buchert, H. Kutz, L. Rossa, O. Sauer, M. Fromme, D. Wallacher, K. Kiefer, and K. Rolfs, Upgrade project NEAT2016 at Helmholtz Zentrum Berlin - What can be done on the medium power neutron source, *Phys. B* **551**, 506 (2018).
- [26] K. Koepernik and H. Eschrig, Full-potential nonorthogonal local-orbital minimum-basis band-structure scheme, *Phys. Rev. B* **59**, 1743 (1999).
- [27] J. Perdew, K. Burke, and M. Ernzerhof, Generalized Gradient Approximation Made Simple, *Phys. Rev. Lett.* **77**, 3865 (1996).
- [28] D. Johnston, R. Kremer, M. Troyer, X. Wang, A. Klümper, S. Bud'ko, A. Panchula, and P. Canfield, Thermodynamics of spin $S = 1/2$ antiferromagnetic uniform and alternating-exchange Heisenberg chains, *Phys. Rev. B* **61**, 9558 (2000).
- [29] V. Laguta, M. Buryi, A. Beitlerova, O. Laguta, K. Nejezchleb, and M. Nikl, Vanadium in yttrium aluminum garnet: Charge states and localization in the lattice, *Opt. Mater.* **91**, 228 (2019).
- [30] A. Abragam and B. Bleaney, Electron paramagnetic resonance of transition ions, in *Oxford Classic Texts in the Physical Sciences* (Oxford University Press, Oxford, 2012).
- [31] J. Bonner and M. Fisher, Linear magnetic chains with anisotropic coupling, *Phys. Rev.* **135**, A640 (1964).
- [32] H. Xiang, E. Kan, S. Wei, M. Whangbo, and X. Gong, Predicting the spin-lattice order of frustrated systems from first principles, *Phys. Rev. B* **84**, 224429 (2011).
- [33] A. Tsirlin, Spin-chain magnetism and uniform Dzyaloshinsky-Moriya anisotropy in BaV_3O_8 , *Phys. Rev. B* **89**, 014405 (2014).
- [34] A. Saúl and G. Radtke, Density functional approach for the magnetism of $\beta\text{-TeVO}_4$, *Phys. Rev. B* **89**, 104414 (2014).
- [35] F. Weickert, N. Harrison, B. Scott, M. Jaime, A. Leitmäe, I. Heinmaa, R. Stern, O. Janson, H. Berger, H. Rosner, and A. Tsirlin, Magnetic anisotropy in the frustrated spin-chain compound $\beta\text{-TeVO}_4$, *Phys. Rev. B* **94**, 064403 (2016).
- [36] A. Tsirlin, R. Nath, J. Sichelschmidt, Y. Skourski, C. Geibel, and H. Rosner, Frustrated couplings between alternating spin-1/2 chains in AgVOAsO_4 , *Phys. Rev. B* **83**, 144412 (2011).
- [37] R. Nath, A. Tsirlin, E. Kaul, M. Baenitz, N. Büttgen, C. Geibel, and H. Rosner, Strong frustration due to competing ferromagnetic and antiferromagnetic interactions: Magnetic properties of $M(\text{VO})_2(\text{PO}_4)_2$ ($M = \text{Ca}$ and Sr), *Phys. Rev. B* **78**, 024418 (2008).
- [38] M. Roca, P. Amorós, J. Cano, M. Dolores Marcos, J. Alamo, A. Beltrán-Porter, and D. Beltrán-Porter, Prediction of magnetic properties in oxovanadium(IV) phosphates: The role of the bridging PO_4 anions, *Inorg. Chem.* **37**, 3167 (1998).
- [39] G. Nilsen, A. Raja, A. Tsirlin, H. Mutka, D. Kasinathan, C. Ritter, and H. Rønnow, One-dimensional quantum magnetism in the anhydrous alum $\text{KTi}(\text{SO}_4)_2$, *New J. Phys.* **17**, 113035 (2015).
- [40] J. Leiner, J. Oh, A. Kolesnikov, M. Stone, M. Le, E. Kenny, B. Powell, M. Mourigal, E. Gordon, M. Whangbo, J. Kim, S. Cheong, and J. Park, Magnetic excitations of the Cu^{2+} quantum spin chain in $\text{Sr}_3\text{CuPtO}_6$, *Phys. Rev. B* **97**, 104426 (2018).
- [41] A. Abdeldaim, A. Tsirlin, J. Ollivier, C. Ritter, D. Fortes, R. Perry, L. Clark, and G. Nilsen, One-dimensional quantum magnetism in the $S = 1/2$ Mo(V) system, KMoOP_2O_7 , *Phys. Rev. B* **107**, 014415 (2023).
- [42] R. Coldea, D. Tennant, and Z. Tylczynski, Extended scattering continua characteristic of spin fractionalization in the two-dimensional frustrated quantum magnet Cs_2CuCl_4 observed by neutron scattering, *Phys. Rev. B* **68**, 134424 (2003).
- [43] M. Kohno, O. Starykh, and L. Balents, Spinons and triplons in spatially anisotropic frustrated antiferromagnets, *Nat. Phys.* **3**, 790 (2007).
- [44] A. Garrett, S. Nagler, D. Tennant, D. Sales, and T. Barnes, Magnetic Excitations in the $S = 1/2$ Alternating Chain Compound $(\text{VO})_2\text{P}_2\text{O}_7$, *Phys. Rev. Lett.* **79**, 745 (1997).
- [45] D. A. Tennant, S. Nagler, A. Garrett, T. Barnes, and C. Torardi, Excitation Spectrum and Superexchange Pathways in the Spin Dimer $\text{VODPO}_4 \cdot 1/2\text{D}_2\text{O}$, *Phys. Rev. Lett.* **78**, 4998 (1997).
- [46] F. Weickert, A. Aczel, M. Stone, V. Garlea, C. Dong, Y. Kohama, R. Movshovich, A. Demuer, N. Harrison, M. Gamza, A. Steppeke, M. Brando, H. Rosner, and A. Tsirlin, Field-induced double dome and Bose-Einstein condensation in the crossing quantum spin chain system AgVOAsO_4 , *Phys. Rev. B* **100**, 104422 (2019).